Astronomy Reports, Vol. 48, No. 8, 2004, pp. 678–687. Translated from Astronomicheskiĭ Zhurnal, Vol. 81, No. 8, 2004, pp. 746–756.

Solar Magnetic Fields and the Intensity of the Green Coronal Line

O. G. Badalyan and V. N. Obridko

Institute of Terrestrial Magnetism, Ionosphere, and Radiowave Propagation, Russian Academy of Sciences, Troitsk, Moscow oblast, 142190 Russia

Received December 25, 2003; in final form, January 9, 2004

Abstract—Synoptic maps of the intensity of the λ530.5 nm FeXIV green coronal line and maps of computed coronal magnetic fields for the period 1977–2001 are compared. For quantitative comparisons, the correlation coefficients r for the correlation between these two parameters at corresponding points of the synoptic maps are calculated. This coefficient exhibits cyclic variations in the spot-formation zone, ±30° and the zone above 30° and is in antiphase in these two zones. In the low-latitude zone, the correlation coefficient is always positive, reaches its maximum at activity minimum, and strongly decreases by activity maximum. Above 30°, r reaches maximum positive values at activity maximum and then gradually decreases, passing through zero near the beginning of the phase of activity minimum and becoming negative during this phase. A Fourier analysis of r as a function of time reveals a wavelike variation with a period close to 1.3 yr (known also from helioseismological data for the tachoclinic region of magnetic-field generation), as well as a pronounced wave with a period of about 5 yr. The latitude dependence of r seems to be related to variations in the contributions from local, large-scale, and global fields. Our analysis suggests an approach to studying the complex problem of mechanisms for coronal heating. © *2004 MAIK "Nauka/Interperiodica"*.

1. INTRODUCTION

It is quite clear that the activity of the Sun and stars of late spectral types similar to the Sun is undoubtedly related to magnetic fields. In the absence of magnetic fields, stars would be "lifeless" spheres without appreciable manifestations of activity. However, the magnetic fields have different relations to different active processes, and the mechanisms for these relationships have not been fully studied. To elucidate the influence of the magnetic field on physical processes in the corona, the relationships between various indices and the magnetic field must be quantitatively evaluated. Such studies that are also based on reasonably extensive statistical data are small in number.

One very important index of solar activity is the intensity of the so-called green coronal line. This is the FeXIV λ 530.5 nm forbidden line, which is formed in the lower corona at a temperature of ~2 MK. Its emission characterizes the level of activity in the solar corona, which is, in turn, related to the activity of underlying layers of the solar atmosphere. The regions of brightest emission in the green line are dense loops and loop clusters, since the intensity of this line is proportional to the square of the density. The existence of such regions is associated with coronal magnetic fields and related to the general problem of coronal heating. Regions of reduced green-line emission are genetically related to coronal holes [1, 2]. Thus, studies of the spatial and temporal distributions of the green-line brightness and comparison of these distributions with parameters of the magnetic field provide a very promising tool for analyzing variations in solar activity and mechanisms for coronal heating.

One big advantage of the index characterizing the green-line emission is that it can be determined almost simultaneously for all heliographic latitudes. This makes it possible to analyze solar activity based on uniform data for the entire solar surface. Thus, this index can provide a uniform and continuous digital field for all points on the disk over long time intervals. In this respect, it stands out, for example, from the Wolf number describing low-latitude activity or the number of polar (high-latitude) facula.

The currently available series of systematic observations of the green coronal line covers almost six solar-activity cycles. These observations have been carried out by a small number of coronal stations, with each of them operating in its own photometric scale. This makes it difficult to combine all available observations into a single system. We will use here the database prepared by Sýkora [3–5].

Since the green-line emission is very closely related to magnetic fields on various scales, studies of the time evolution of the spatial-intensity distribution in the green corona can be used to trace the evolution of coronal magnetic fields. It is especially important in this context that the intensity of the green coronal

1063-7729/04/4808-0678$26.00

line can be directly measured, in contrast to the parameters of the coronal magnetic field, which can only be calculated based on photospheric observations applying certain assumptions. We also emphasize that detailed and systematic observations of photospheric magnetic fields cover a substantially shorter time interval than do observations of the green line. Therefore, conclusions derived from joint investigations of magnetic fields and the emission in the green coronal line can be extrapolated to past times when magnetic-field measurements were obtained only episodically and on various scales.

Unfortunately, few direct comparisons between the parameters of coronal-line emission and the magnetic field have been carried out. We note in this context the paper of Guhathakurta *et al.* [6], who made such comparisons based on data for 1984–1992. They calculated the coronal temperature from the ratio of the intensities of the red (λ637.4 nm FeX) and green (λ530.3 nm FeXIV) lines and then compared this temperature with the white-corona emission and the line-of-sight component of the photospheric magnetic field measured at the Kitt Peak Observatory. The temperature distribution obtained in [6] is very different from the magnetic-field distribution. The spatial and temporal distributions of the green- and red-corona brightnesses are more interesting. The distribution of the green-corona emission fairly closely resembles the distribution of the magnetic field. In particular, midlatitude bands in which the magnetic-field strength and coronal-line intensities increase can be noted in the growth phase of the cycle in both hemispheres. As the maximum of the cycle is approached, these bands expand toward both high and low latitudes, with a single equatorial band forming toward the cycle minimum.

A different technique for comparing the emission in the green coronal line with magnetic-field parameters was employed by Wang *et al.* [7], who analyzed data from the SOHO LASCO C1 coronagraph obtained over five days. The structure of the magnetic field lines was calculated in a potential approximation using data of the Stanford Wilcox Solar Observatory. The structures of the magnetic field and green-line emission agreed well. It was shown that the density at the base of magnetic flux tubes is related to the strength of the magnetic field as $n_{foot} \propto \langle B_{foot} \rangle^{0.9}$.

Fairly extensive soft X-ray and EUV observations of the solar disk have now been accumulated. Yohkoh, SOHO, Trace, and CORONAS images of the corona cover a period of about one activity cycle, from 1991. Such observations make it possible to compare coronal images obtained in various X-ray lines with daily observational maps of the magnetic field. However, these spacecraft have different equipment, resulting in nonuniformity of the observational material and, accordingly, in some problems with such comparisons.

The radiation at λ195 Å FeXII recorded on the spacecraft is emitted by virtually the same regions where the green coronal line is emitted. Images taken in this line show that the coronal emission is enhanced above active regions and reduced above coronal holes. Comparisons of green-line synoptic maps with short-wavelength coronal images [8] show that they are in good agreement. Discrepancies seem to be due to transient phenomena that are not reflected in the synoptic maps.

Our previous analysis of the spatial and temporal distributions of the green coronal-line intensity for 1943–2001 [8] confirmed that the green-corona brightness is largely determined by the strength of the coronal magnetic field for this long time interval. There was good agreement in the spatial structures of several synoptic maps of the green-corona brightness and maps of the coronal magnetic field at the heights of the green-line emission during the decline phase of activity cycle 21. This led us to conclude that the green-line intensity and the strength of the coronal magnetic field are, in general, positively correlated at low latitudes. In addition, we tested in [8] a technique for quantitatively estimating correlations between synoptic maps of the green-line intensity and the coronal magnetic field.

Here, we present a detailed comparison between synoptic maps of the green-line intensity and of the magnetic field for 1977–2001 (activity cycles 21, 22, and 23—the current cycle). For quantitative comparisons, we calculated the correlation coefficients between the green-line intensity and magnetic-field strength at corresponding points of the green-corona and magnetic-field synoptic maps. The calculations were done for both the entire latitude range $\pm 70°$ for which the magnetic field is computed and for individual latitude zones. This analysis makes it possible to draw certain conclusions about the extent to which magnetic fields on various scales affect the green-corona emission at various phases of the solar activity cycle. This approach enables us to closely approach a solution to the very complex problem of coronal-heating mechanisms.

2. THE MATERIAL USED

2.1. Database of Intensities of the Green Coronal Line

Monitoring observations of the FeXIV λ 530.5 nm green coronal line were initiated in 1939 at the Pic du Midi and Arosa stations. During the first several years, test observations were carried out, and observational data are available for only a few days

of those years. Later, systematic observations were started on a small network of coronal stations, and the yearly number of observational days increased. However, different stations employed different observational techniques based on inevitably different photometric scales, and carried out their measurements at different heights over the limb. This raised the nontrivial task of reducing the observations of different stations to a unified system. Some issues related to this procedure are considered in detail by Sýkora [3–5].

Several photometrically uniform databases of green-corona intensities are available, which differ mainly in their choice of the coronal station adopted as a photometric standard [1, 9, 10]. We use here the database compiled by J. Sýkora (Slovak Republic); a detailed description of this database can be found in [11]. The observations are represented in the form of an array in which the intensities of the green line along the solar limb are given for each day in position-angle steps of 5°. Thus, synoptic maps with a resolution of $\sim 13°$ in longitude and 5° in latitude can be directly constructed from the observational data. The green-line intensity is expressed in absolute coronal units (acu, one millionth of the intensity at the solar-disk center within 1 Å in the continuum next to the line) and refers to a height of 60″ above the limb.

The database can be used to consider cyclic variations in the green-line intensity both in the entire latitude range from $+90°$ to $-90°$ and for individual latitude zones, with various time resolutions. This enables one to investigate north–west asymmetries with respect to heliographic latitude, study the brightest (active) regions in the corona separately, and examine regions of reduced green-line emission that appear to be related to coronal holes [12]. Analyses of active longitudes and coronal-rotational velocities at various latitudes are also possible [13].

2.2. Calculations of the Coronal Magnetic Field

The coronal magnetic-field strengths were calculated in a potential approximation based on measurements at the photospheric level carried out at the Wilcox Solar Observatory (the data were obtained via the Internet). We used observations of the line-of-sight component of the photospheric magnetic field summarized in synoptic maps for each Carrington rotation as the source data.

We calculated the coronal magnetic field using the widely known method described in [14, 15] and employed a code that allows the calculation of all components of the magnetic field everywhere from the photospheric surface to the source surface [16, 17]. Synoptic maps of these components can be calculated for any selected time that is taken as the position of the central meridian. For the subsequent analysis, we calculated the total magnetic-field strength B (the square root of the sum of the squares of the radial, B_r, and tangential, B_t, components) at a height of $1.1R_\odot$, which roughly corresponds to the data for the green coronal line. The calculations summed over ten harmonics and introduced a polar correction to take into account the lower reliability of magnetic-field measurements near the poles [18]. Both the original and calculated data on the magnetic field are restricted to the latitude range $\pm 70°$.

3. COMPARISONS BETWEEN THE SYNOPTIC MAPS OF THE GREEN-LINE INTENSITY AND CORONAL MAGNETIC FIELDS

Cyclic variations in the brightness distribution of the green coronal line were considered in [8] based on synoptic maps for 1943–2001 subjected to a running average over six Carrington rotations with a step of one rotation. Such synoptic maps make it possible to trace gradual changes in the spatial distribution of the brightness of the green coronal line during the solar activity cycle. Smoothing over six Carrington rotations enables more reliable identification of long-lived features on fairly large scales.

Similar synoptic maps were also constructed for the magnetic-field strength. The maps calculated for each Carrington rotation were averaged over six rotations with a step of one rotation. All the calculations were done for a distance of 1.1 $R_\odot$.

Figure 1 presents three pairs of synoptic maps for the magnetic-field strength in μT (upper row) and the green-line intensity in acu (lower row). In a given map, the chosen range for the quantity displayed is divided into eight gradations, with the largest values shown as black, and the smallest, as white. Not all eight gradations are always shown in a map, in order to make clearer cyclic variations in the parameters studied (for example, the decreases in the green-line brightness at the activity minimum). In particular, white is missing in the first and second maps of the lower row (green line), and the two highest gradations of black are missing from the third map of the same row. The contours delimiting the darkest areas correspond to 240, 480, and 280 μT in the upper row of maps (from left to right) and to 150, 170, and 40 acu in the lower row of maps. Thus, the contour increments are 30, 60, and 35 μT for the maps in the upper row and 18.75, 13.75, and 5 acu for the maps in the lower row. The horizontal and vertical axes plot heliographic longitude and latitude, and time runs from left to right. The heading over any pair of maps indicates the corresponding averaging interval.

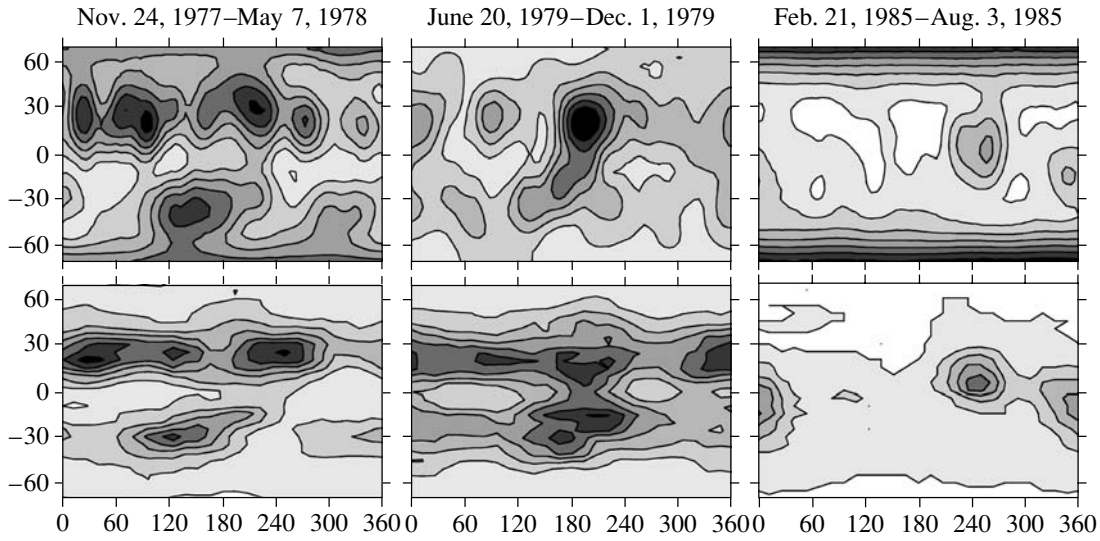

Fig. 1. Comparison of synoptic maps of the magnetic-field strength (top) and green-line intensity (bottom). The magnetic-field strength is measured in μT, and the green-line intensity, in acu. In each map, the total range of the corresponding quantities is divided into eight gradations, so that the largest values are shown as black, and the smallest, as white. The contour increments (from left to right) are 30, 60, and 35 μT for maps in the top row and 18.75, 13.75, and 5 acu for maps in the bottom row. Longitude is plotted along the horizontal axis, and latitude, along the vertical axis, and time runs from right to left.

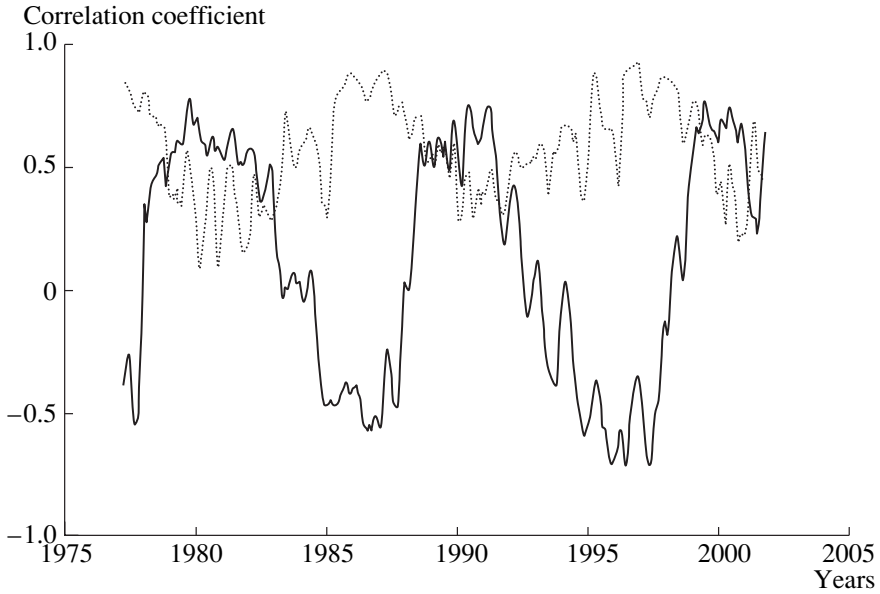

Fig. 2. Time variations in the correlation coefficient r for the correlation between the magnetic-field strength and the intensity of the green line measured at spatially coincident points of the maps in the spot-formation zone, $\pm 30°$ (dotted curve), and at high latitudes, above 30° (solid curve).

The maps in Fig. 1 were constructed for various phases of cycle 21. The left pair of maps refers to the growth phase of the activity cycle. We can see that the green-line intensity and the magnetic-field strength are generally in good agreement. Regions of both large and small values of the corresponding parameters coincide well, especially in the low-latitude spot-formation zone. The next pair of maps corresponds to a time interval near the cycle maximum. Here, the agreement between the maps is worse for the spot-formation zone and better for the higher latitudes. The third pair of maps was constructed for a period near the minimum of the activity cycle. The intensity of the green coronal line is substantially reduced, and the magnetic field is much more uniform (less structured). However, the rela-

tively rare regions of enhanced magnetic fields in the low-latitude zone (sometimes, there is only one such region) normally coincide with regions of enhanced green-line emission. At the same time, a negative correlation between the green-line intensity and the magnetic-field strength can be noted at high latitudes. The field strength increases toward the poles, substantially exceeding the B values in the equatorial zone; in contrast, the green-line intensity decreases toward the poles. Note that, combined with our Fig. 1, the three pairs of maps for the declining phase of cycle 21 presented in [8] suggest gradual changes in the correspondence between the parameters studied at low and high latitudes during the activity cycle.

To quantify similarities or differences between the synoptic maps, it was suggested in [8] to compute cross-correlation coefficients for corresponding points in maps of the green corona and magnetic fields. For this purpose, the magnetic-field strengths were calculated for those points in the synoptic map for which data on the green line were available; there are 27 such points in longitude (one rotation) and 29 points in latitude (in steps of 5° in the range ±70°, where the magnetic field was calculated). Such cross correlations can be determined both for the entire range of latitude ±70° and for selected, narrower latitude zones.

Even the first estimates based on this technique [8] indicated that the intensity of the green-corona emission is closely related to the magnetic-field strength. However, this relationship depends strongly on the latitude zone and phase of the cycle. The correlation coefficient and even its sign are different in the polar zone and in the low-latitude spot-formation zone. It was concluded that the correlation coefficient for the high-latitude corona (above 30°) increases near the cycle maximum, when the magnetic field at high latitudes is relatively low. Further, as the minimum is approached, the correlation coefficient gradually decreases and changes its sign. This can be seen in Fig. 1.

Here, we present a much more detailed comparison for all available synoptic maps of the green-line intensity and magnetic field. This enables us to trace cyclic changes in the relationship between the green-line intensity and magnetic-field strength in various latitude zones.

Figure 2 displays the time variations of the correlation coefficient, r, for two latitude zones—the spot-formation zone ±30° and a high-latitude zone. The high-latitude zone refers to regions with latitudes exceeding 30° in both the northern and southern hemispheres. First and foremost, we can see that r exhibits cyclic variations in both zones. Further, the r values in the two zones seem to vary in antiphase. In the low-latitude zone, r is always positive, reaching a maximum at the activity minimum and strongly decreasing by the activity maximum. The situation is different at latitudes above 30°. The correlation coefficient r reaches its maximum positive values at the maximum of the activity cycle, after which it gradually decreases, passes through zero, and, by the activity minimum, reaches negative values whose absolute magnitudes are nearly equal to the positive values achieved at activity maximum. At the same time, the absolute values of r at the high latitudes never become as large as they do in the spot-formation zone near minima of the solar-activity cycle. The cross-correlation coefficients for the maps presented in Fig. 1 are (from left to right) 0.812, 0.574, and 0.800 for the zone ±30° and 0.274, 0.755, and −0.458 for the zone above 30°.

The sign change of r at high latitudes coincides with the reference points of the cycle t_{mA} (the beginning of the growth phase) and t_{Dm} (the end of the decline phase and beginning of the minimum phase) to within a few months, so that negative values of r fairly precisely border the phase of minimum activity. (We use here the calendar dates for the reference points determined in [19].)

The spatial and temporal variations in r over the entire latitude range ±70° are shown in Fig. 3. All features of the variations of r with time and latitude can be traced clearly in this diagram. The regions of relatively high positive correlation coefficients, $r \geq 0.5$, span a fairly broad latitude range during periods of solar-activity decline and alternate with small intervals where this r is reduced, also over a broad range of latitudes. The increases in size of the polar region with negative r values occur in a similar wavelike fashion during periods that are close to the solar-activity minimum. It is interesting that there is a latitude zone, 30°−40°, where r is close to 0.5 and exhibits virtually no cyclic variations. This means that zones displaying different behavior of the correlation coefficient are roughly separated by a latitude belt of quiescent filaments.

The nature of the latitude dependence of the correlation coefficient r is probably related to variations in the contributions of the local, large-scale, and global fields, each having their own dependence on the phase of the cycle.

4. DEPENDENCE OF THE CORRELATION COEFFICIENT ON THE PHASE OF THE CYCLE

The time interval for which the cross correlation between the synoptic maps of the green-line intensity and the coronal magnetic-field strength can be studied (in other words, the interval for which the magnetic field can be calculated from the Stanford data)

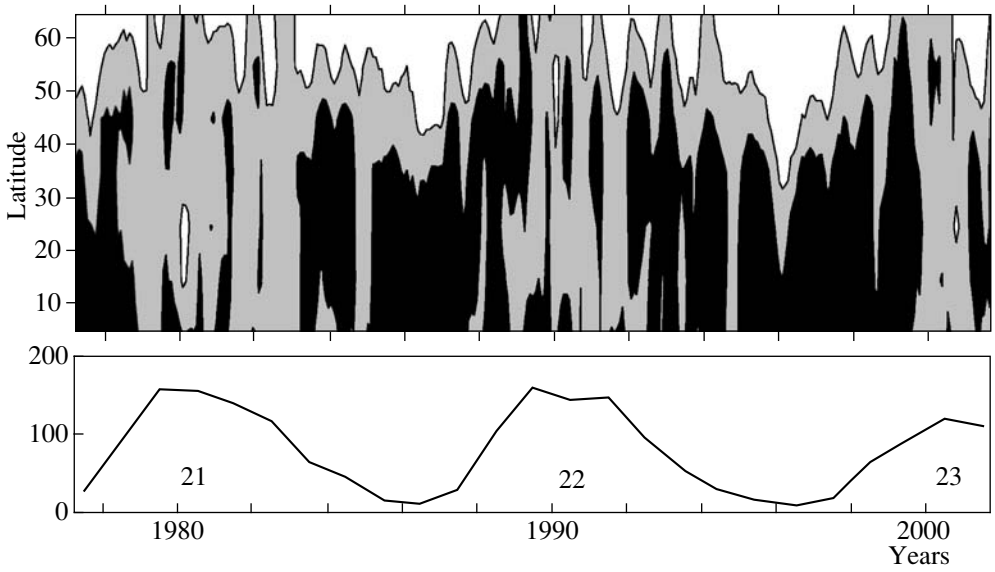

Fig. 3. General latitude–time diagram for the correlation coefficient r. Regions with $r > 0.5$ are shown black; those with $-0.5 < r < 0.5$, gray; and those with $r < -0.5$, white. The bottom panel plots the mean annual Wolf numbers along the vertical axis; the numbers of the corresponding activity cycles are indicated.

encompasses activity cycles 21, 22, and (partially) 23. It is interesting to trace changes in r from cycle to cycle. This can be done by superposing the time variations in r for various cycles on one graph.

Figure 4 shows such a superposition for latitudes $\pm 30°$. The time shift was chosen so that the coincidence (pairwise correlation) of all three curves was best. The year is plotted along the horizontal axis on a scale in which, for the first cycle considered (cycle 21, heavy solid curve), zero corresponds to 1976, and 12, to 1988. The next two cycles (22 and 23) are shifted by one and two chosen time shifts, respectively.

Both Fig. 2 and the general map in Fig. 3 clearly display a certain quasiperiodic component superposed on the overall time variations in r. The Fourier analysis described in detail below shows that this component has a period close to 1.5 yr. The effect of this wave is fairly significant for our choice of the best time shift in Fig. 4. We ultimately took this shift to be 133 Carrington rotations, slightly less than 10 yr. We can see in Fig. 4 both the generally good coincidence in the cyclic variations of r and the agreement of many features associated with the high-frequency component. The correlations between the curves in Fig. 4 for cycles 21 and 22, 21 and 23, and 22 and 23 calculated in the latitude zone $\pm 30°$ for the chosen time shift are 0.755, 0.768, and 0.728, respectively.

We carried out a Fourier analysis to reveal quasiperiodic variations in r more reliably. Calculations were done separately for ten-degree latitude zones and for the entire latitude range. The green-corona brightness and the magnetic-field strength themselves, averaged over six rotations for latitudes $\pm 30°$ and above 30°, were also subjected to a Fourier analysis. The sum of all the squares of the Fourier amplitudes is equal to the standard deviation of the correlation coefficient r from its mean over the time interval studied. The Fourier analysis confirmed the presence of a high-frequency wave (with a period of 1–1.5 yr) in the r values for all latitudes, as well as a fairly pronounced 5-yr wave. Oscillations with periods of 1–1.5 yr and 5 yr are distinctly visible in both r and the indices themselves.

Figure 5 shows a Fourier periodogram for r for all latitudes and the period range 0.5–3 yr. The range of the amplitude variations for oscillations of r was chosen to be 0.015–0.06 and is divided into six gradations; thus, the contour increment in Fig. 5 is 0.0075.

Oscillations with periods of 1–1.5 yr are clearly visible in Fig. 5; oscillations with periods of about 1 yr dominate at high latitudes, while 1.3-yr oscillations dominate at medium and low latitudes. Note that this same period, 1.3 yr, was detected helioseismologically in the tachocline region of the magnetic-field generation [20]. The 1.3-yr oscillations are also distinct at the tachocline level at medium and low latitudes, while these oscillations seem to be weaker or to have a shorter period at high latitudes. The well-known quasi-biennial oscillations are very weak in Fig. 5. Since we are analyzing the correlation coefficient for correlations between the intensity of the green coronal line and the magnetic-field strength, it is natural that not all significant oscillations in these activity indices will be manifest in the correlation between them. In our case, the quasi-biennial oscillations can be easily distinguished in the magnetic-field strength

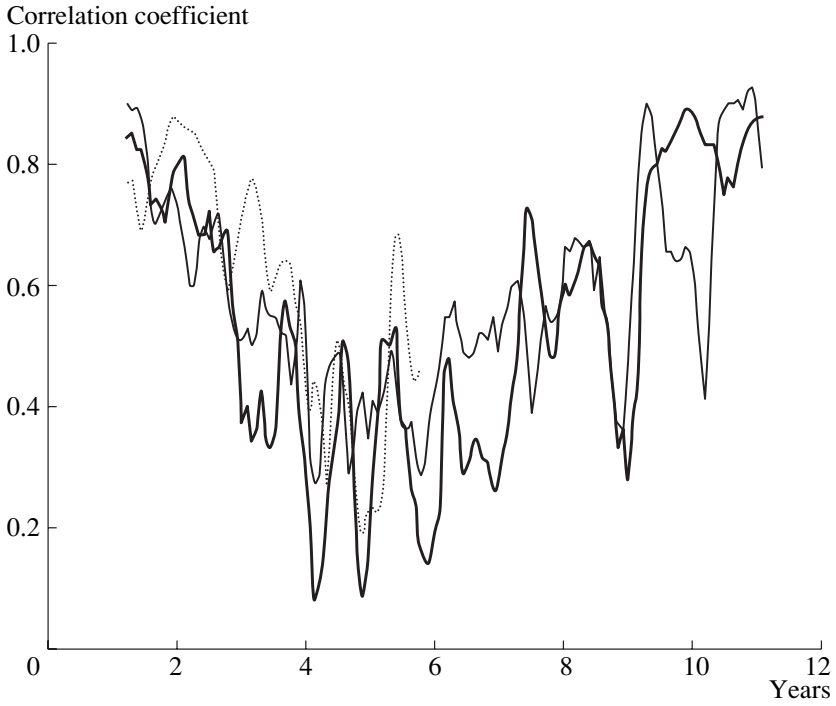

Fig. 4. Time variations in the correlation coefficient r during cycles 21 (heavy solid curve), 22 (light solid curve), and 23 (dotted curve) for latitudes $\pm 30°$. The year is plotted along the horizontal axis on a scale in which zero corresponds to 1976 and 12 corresponds to 1988 for cycle 21, and the scales for cycles 22 and 23 are shifted by 133 and 266 rotations, respectively. The shift by 133 Carrington rotations is chosen to achieve the best pairwise correlation of all three curves. A quasi-annual wave superposed onto the cyclic variations in r is clearly visible in all three curves.

and green-line intensity. These oscillations are even more pronounced in the asymmetry of various solar-activity indices [21, 22].

In contrast to periods of 1–1.5 yr, oscillations in r with periods of about 5 yr gradually increase toward high latitudes (the low-frequency region is not shown in Fig. 5). At middle latitudes, oscillations with this period form a distinct spectral peak.

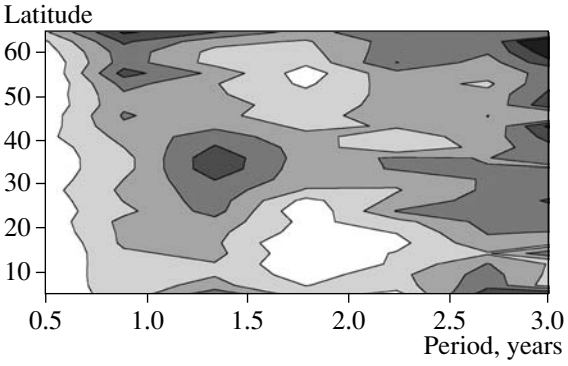

Fig. 5. Fourier periodogram of the correlation coefficient r for periods from 0.5 to 3 yr. The contour increment for variations in the amplitude of r is 0.0075. Oscillations in the range 1–1.5 yr are clearly visible, while the quasi-biennial oscillations are very weak.

At higher latitudes, this peak gradually changes on its low-frequency side into a general increase in the oscillation amplitude right up to the 11-yr period. At low latitudes, the 5-yr oscillations are relatively weak, and the oscillation amplitude gradually grows at low frequencies.

The low-frequency part of the Fourier spectrum of the correlation coefficient is substantially weakened at latitudes of 30°–40°. This agrees with the fact that, as was noted above in the discussion of Fig. 3, the 11-yr cycle is weakly expressed in the behavior of the correlation coefficient at these latitudes.

Figure 6 represents r for the correlation between the coronal magnetic-field strength and the intensity of the green coronal line as a function of the cycle phase. The cycle phase here is calculated according to [23], as $\Phi = (T - m)/(|M - m|)$, where T is the current time and M and m are the times of the nearest maximum and minimum of the 11-yr cycle, respectively. According to this definition, the phase is zero at the cycle minimum, positive on the ascending branch of the cycle, and negative on the descending branch.

Figure 6 most clearly displays overall variations in r with the cycle phase for the spot-formation zone (upper curve, open circles) and the zone above 30° (lower curve, solid circles). All the features of the time

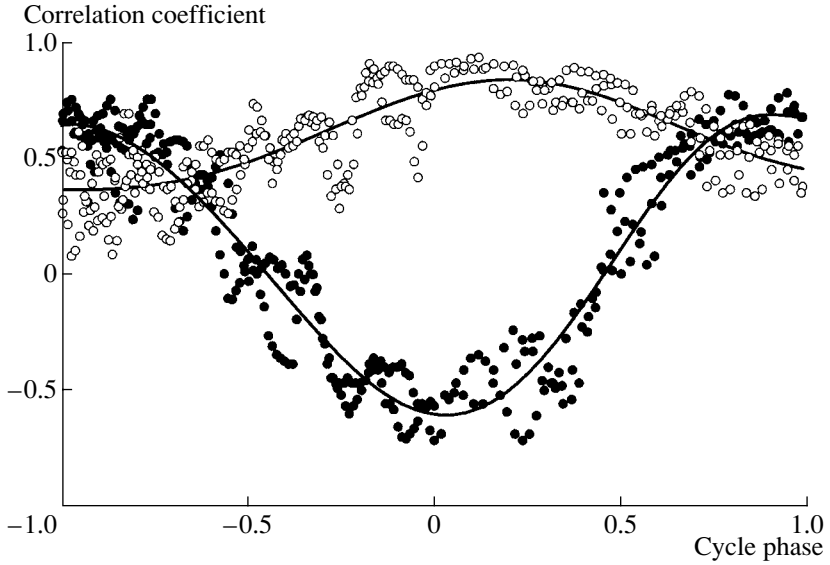

Fig. 6. Variation in the correlation coefficient r with phase of the cycle for the spot-formation zone (upper curve, open circles) and the zone above 30° (lower curve, solid circles).

variations of r in these two latitude zones discussed above are clearly visible in this figure. The mean correlation coefficient in the spot-formation zone varies from ≈ 0.35 at the activity maximum to ≈ 0.85 at the minimum, and it varies in the high-latitude zone from ≈ 0.6 to ≈ -0.6. The effect of the high-frequency wave is also appreciable, leading to corresponding departures of the actual variations in r from the solid curves approximating the cyclic variations in r.

Figure 7 presents the relationship between r and the magnetic-field strength itself at a height of 1.1 $R_\odot$ for latitudes ±30° (upper panel) and latitudes above 30° (lower panel). The following features can be noted. Most importantly, there is a decrease in r with increasing magnetic-field strength in the spot-formation zone and, vice versa, an increase in r with B at latitudes above 30°. The magnetic field itself in the spot-formation zone varies dramatically during a cycle, by a factor of 10–15, and approaches values $B \sim 20$ μT at the cycle minimum. Recall that this is the field averaged over six Carrington rotations for the given latitude zone. At higher latitudes (lower graph), the mean magnetic field varies much less during the cycle, by only a factor of 1.5–2, reaching 70–100 μT at the activity maximum (negative values of r) and no more than 200 μT at the activity minimum.

A joint consideration of Figs. 6 and 7 clearly shows that the green-line intensity in the spot-formation zone is most closely related to the magnetic-field strength near the activity minimum. The field in the spot-formation zone decreases and becomes more ordered, and the enhancement of the field in some regions results in a corresponding enhancement of the green-line emission. In contrast, the field at high latitudes increases as the minimum is approached, while the intensity of the green line decreases (Fig. 1).

At activity maximum, when the low-latitude magnetic field is strong, there is no such relation, as is reflected by a substantial decrease in r. We should emphasize that the general cyclic variations in both the green-line intensity and the magnetic-field strength in the spot-formation zone correspond well with the well-known Wolf-number curve. In contrast, the field strength for latitudes above 30° is in antiphase with the Wolf numbers, while the intensity of the green line continues to follow the cyclic Wolf-number curve.

Thus, Fig. 6 and, especially, Fig. 7 indicate that the relationship between the green-line intensity and the coronal magnetic field is not determined by a single universal law. The magnetic fields on various scales influence the brightness of the green corona in different ways.

5. CONCLUSIONS

We have made a detailed comparison between synoptic maps of the intensity of the λ530.5 nm green coronal line and the strength of the coronal magnetic field for 1977–2001 (activity cycles 21, 22, and 23, the current cycle). Maps of the green coronal-line intensity were constructed using a photometrically uniform database [3, 11], applying a running average over six Carrington rotations in steps of one rotation, making it possible to reveal large-scale, long-lived features. The magnetic-field strength was calculated from measurements of the line-of-sight field component at the photospheric level carried out at the Stanford John Wilcox Observatory. The calculations

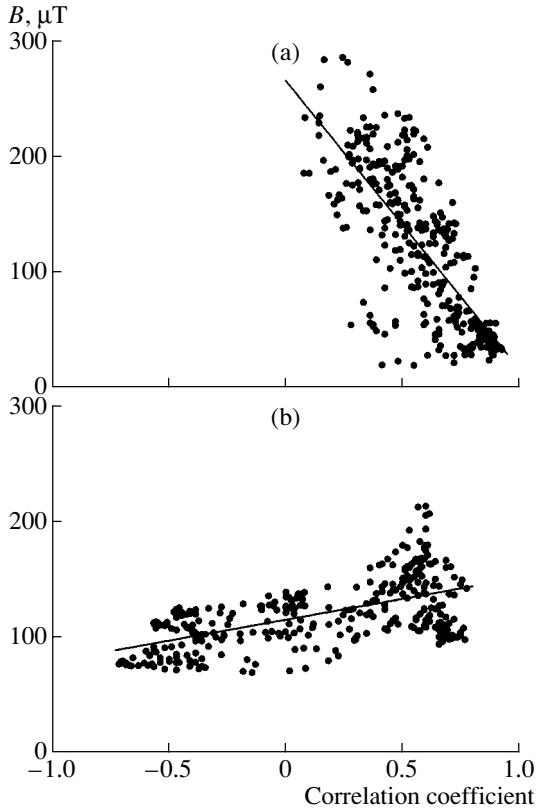

Fig. 7. Relationship between r and the magnetic-field strength in the spot-formation zone (upper panel) and the zone above 30° (lower panel).

were done for a distance of 1.1 $R_\odot$ in a potential approximation for latitudes within ±70°, and the resulting synoptic maps were likewise averaged over six rotations with a step of one rotation.

To quantify the comparison of the green-line intensity and magnetic-field strength in each pair of maps, we calculated the correlation coefficient r for the correlation between these parameters at points of the synoptic maps for which measurements of the green-line intensity were available. This correlation coefficient was calculated for the entire latitude range ±70°, for narrow ten-degree zones, and for the spot-formation zone ±30° and high latitudes above 30°.

We found that r varies cyclically in zones of both low and high latitudes. There are virtually no such cyclic variations between these zones, at latitudes of 30°–40°, close to the zone of quiet filaments. The correlation coefficients r in the spot-formation zone ±30° and at latitudes above 30° vary in antiphase. In the low-latitude zone, r is always positive, reaches maximum values at the activity minimum, and decreases strongly by the activity maximum. In contrast, at latitudes above 30°, r reaches its maximum positive values at the maximum of the activity cycle, after which it gradually decreases and becomes negative by the phase of activity minimum.

The correlation coefficient r increases with the magnetic-field strength in the spot-formation zone and decreases at latitudes above ±30°. The magnetic-field strength averaged over six Carrington rotations varies by a factor of 10–15 in the spot-formation zone and reaches values of $B \sim 20\ \mu$T at the activity-cycle minimum. At latitudes above ±30°, the magnetic field varies by, on average, only a factor of 1.5–2 during the activity cycle, always remaining in the range 50–60 μT at the activity maximum and not exceeding 200 μT at the phase of activity minimum.

A Fourier analysis of the time variations in r reveals a wave with a period close to 1.3 yr; the period of this wave is reduced somewhat at higher latitudes. Helioseismological data likewise indicate 1.3-yr variations in the tachocline region of magnetic-field generation at middle and low latitudes. A 5-yr period also stands out in the Fourier spectrum of the oscillations of r. The amplitude of the oscillations is considerably reduced at latitudes of 30°–40°, while the 11-yr cycle is clearly expressed at higher and lower latitudes.

The dependence of r on the cycle phase provides direct evidence for differences in the influence of fields on various scales on the coronal intensity. As can easily be shown, a universal linear relationship between the magnetic field and the coronal intensity would imply that there should be no dependence of r on the mean magnetic-field strength and, therefore, on the phase of the cycle. If the relationship is nonlinear, r can vary, but only within narrow limits. In our case, however, not only cyclic variations but also changes in the sign of r are observed at high latitudes. This testifies to the action of different mechanisms for the formation of the corona for magnetic fields on small, medium, and large scales. Our results can be used to quantitatively test various models for coronal heating.

The simplest pattern is observed at the cycle minimum, when the large-scale, quasi-dipolar magnetic field at the poles of the Sun reaches a maximum. Polar coronal holes are present in the corona. The coronal intensity and magnetic-field strength at the poles vary in antiphase. In the equatorial zone, the large-scale field virtually disappears, and only isolated complexes of local activity remain. The relationship between the coronal brightness and magnetic fields in the equatorial zone is especially clearly expressed during this period, and the correlation coefficient r reaches a maximum.

The situation is much more complex at activity maximum. Local magnetic fields spread to relatively high latitudes, and tongues of large-scale field (accompanied by coronal holes) penetrate into the equatorial region. Fields on intermediate characteristic scales (the background and floccular fields, loops over

large-scale neutral lines) are clearly expressed. Furthermore, ephemeral active regions living one to three days, which affect the physical processes occurring in the corona but are not reflected in synoptic maps of the magnetic field, as well as nanoflares, are manifest most effectively at the phase of activity maximum. This substantially reduces r in the equatorial zone during the period of cycle maximum.

Thus, the relationship between the magnetic field and the brightness of the green corona and, therefore, the mechanisms for coronal heating seem to be different for fields on different scales. In relatively small-scale fields (local fields) at low latitudes, the heating of the corona is controlled by low flux tubes and nonstationary processes in and near these tubes. Because the magnetic field at the cycle maximum is a complex mixture of arches and loops with various heights and a very complex configuration, the correlation coefficients r cannot be large, even though the brightness of the green corona increases with the field strength. Such a mixture of variously scaled fields is also present at higher latitudes. As the minimum is approached, the field structure becomes more ordered at both high and low latitudes, individual activity complexes emerge in the spot-formation zone, and extended regions of large-scale field appear at high latitudes. The correlation coefficient r increases everywhere, but the relationship between the magnetic-field strength and the green-line intensity is opposite in sign for these latitude zones.

This simple scheme describes the general cyclic behavior of the relationship between the green coronal-line emission and the magnetic-field strength but cannot naturally explain some details. The interpretation of a number of finer effects revealed by our analysis must be elaborated more carefully and in greater detail.

ACKNOWLEDGMENTS

We are grateful to J. Sýkora for discussions of certain points touched upon in this paper. This work was supported by the Russian Foundation for Basic Research (project no. 02-02-16199) and INTAS (grant 2000-840).

REFERENCES

1. J. Sýkora, Solar Phys. **140**, 379 (1992).
2. V. Letfus, L. Kulčár, and J. Sýkora, in *Solar and Interplanetary Dynamics*, Ed. by M. Dryer and E. Tandberg-Hanssen (Reidel, Dordrecht, 1980), p. 49.
3. J. Sýkora, Bull. Astron. Inst. Czec. **22**, 12 (1971).
4. J. Sýkora, Contrib. Astron. Obs. Skalnaté Pleso **22**, 55 (1992).
5. V. Lelfus and J. Sýkora, *Atlas of the Green Corona Synoptic Charts for the Period 1947–1976* (Veda, Bratislava, 1982).
6. M. Guhathakurta, R. R. Fisher, and R. C. Altrock, Astrophys. J. **414**, L145 (1993).
7. Y.-M. Wang, N. R. Sheeley, Jr., S. H. Hawley, *et al.*, Astrophys. J. **485**, 419 (1997).
8. O. G. Badalyan, V. N. Obridko, and J. Sýkora, Solar Phys. (submitted).
9. R. N. Ikhsanov and V. G. Ivanov, in *Proceedings of the Conference on The Sun During the Magnetic Field Mark Change*, Ed. by V. I. Makarov and V. N. Obridko (Gos. Astron. Obs., 2001), p. 175.
10. A. G. Tlatov, S. A. Guseva, and Kim Gunder, in *Proceedings of the Conference on The Sun During the Magnetic Field Mark Change*, Ed. by V. I. Makarov and V. N. Obridko (Gos. Astron. Obs., 2001), p. 385.
11. O. G. Badalyan, V. N. Obridko, and J. Sýkora, Solar Phys. **199**, 421 (2001).
12. L. Kulčár and J. Sýkora, Contrib. Astron. Obs. Skalnaté Pleso **24**, 79 (1994).
13. J. Sýkora, Adv. Space. Res. **14** (4), 73 (1994).
14. J. T. Hoeksema and P. H. Scherrer, *The Solar Magnetic Field—1976 through 1985*, WDCA Report UAG-94, NGDC, Boulder (1986).
15. J. T. Hoeksema, *Solar Magnetic Fields—1985 through 1990*, Report CSSA-ASTRO-91-01 (1991).
16. K. G. Ivanov and A. P. Kharshiladze, Geomagn. Aeron. **34**, 22 (1994).
17. J. Sýkora, O. G. Badalyan, and V. N. Obridko, Solar Phys. **212**, 301 (2003).
18. V. N. Obridko and B. D. Shelting, Solar Phys. **184**, 187 (1999).
19. V. N. Obridko and B. D. Shel'ting, Astron. Zh. **80**, 1034 (2003) [Astron. Rep. **47**, 953 (2003)].
20. R. Howe, J. Christensen-Dalsgaard, F. Hill, *et al.*, Science **287**, 2456 (2000).
21. O. G. Badalyan, V. N. Obridko, J. Rybák, and J. Sýkora, in *Proceedings of the ISCS 2003 Symposium on Solar Variability as an Input to the Earth's Environment*, ESA SP-535, Ed. by A. Wilson (Noordwijk, Netherlands, 2003), p. 63.
22. O. G. Badalyan and V. N. Obridko, in *Proceedings of the Conference on Climatic and Ecological Dimensions of Solar Activity*, Ed. by V. I. Makarov and V. N. Obridko (Gos. Astron. Obs. Ross. Akad. Nauk, St. Petersburg, 2003), p. 33.
23. S. A. Mitchell, Handb. Astrophys. **4**, 231 (1929).

Translated by A. Getling